

Role of axial $U(1)$ anomaly in chiral susceptibility of QCD at high temperature

JLQCD Collaboration: S. Aoki¹, Y. Aoki², H. Fukaya³, S. Hashimoto⁴,
C. Rohrhofer⁵, and K. Suzuki⁶

¹ *Center for Gravitational Physics, Yukawa Institute for Theoretical Physics, Kyoto University, Kyoto 606-8502, Japan*

² *RIKEN Center for Computational Science, 7-1-26*

Minatojima-minami-machi, Chuo-ku, Kobe, Hyogo 650-0047, Japan

³ *Department of Physics, Osaka University, Toyonaka 560-0043, Japan*

⁴ *High Energy Accelerator Research Organization (KEK), Tsukuba 305-0801, Japan*

⁴ *School of High Energy Accelerator Science, The Graduate University for Advanced Studies (Sokendai), Tsukuba 305-0801, Japan*

⁵ *Department of Physics, Osaka University, Toyonaka 560-0043, Japan*

⁶ *Advanced Science Research Center, Japan Atomic Energy Agency (JAEA), Tokai 319-1195, Japan*

.....
The chiral susceptibility, or the first derivative of the chiral condensate with respect to the quark mass, is often used as a probe for the QCD phase transition since the chiral condensate is an order parameter of $SU(2)_L \times SU(2)_R$ symmetry breaking. However, the chiral condensate also breaks the axial $U(1)$ symmetry, which is usually not paid attention to as it is already broken by anomaly and apparently gives little impact on the transition. We investigate the susceptibilities in the scalar and pseudoscalar channels in order to quantify how much the axial $U(1)$ breaking contributes to the chiral phase transition. Employing a chirally symmetric lattice Dirac operator, and its eigenmode decomposition, we separate the axial $U(1)$ breaking effects from others. Our result in two-flavor QCD indicates that both of the connected and disconnected chiral susceptibilities are dominated by the axial $U(1)$ breaking at temperatures $T \gtrsim 190$ MeV after the quadratically divergent constant is subtracted.

1 Introduction

Properties of phase transition are largely governed by symmetries that are broken/restored at the transition. In Quantum Chromodynamics (QCD) with two degenerate dynamical quarks (up and down), the relevant symmetry is that of flavor rotation of left- and right-handed quark fields, *i.e.* $SU(2)_L \times SU(2)_R$ chiral symmetry, which is spontaneously broken at low temperatures but is believed to be recovered at some high temperature our universe experienced at its early stage. The chiral condensate $\Sigma(m) = -\sum_x \langle S^0(x) \rangle / V$, defined with a flavor singlet scalar quark bilinear operator $S^0(x)$ and the four-volume V , as well as its derivative $\chi(m) = \frac{\partial}{\partial m} \Sigma(m)$ known as the chiral susceptibility, are often used to probe the so-called chiral phase transition [1–9].

The condensate also breaks the flavor-singlet axial symmetry $U(1)_A$ but its relevance is not immediately clear, since it is broken by quantum anomaly, which exists at any energy scale. The $U(1)_A$ anomaly may still affect the low-energy dynamics as it is related to the topology of the gluon field and the zero eigenstates of the Dirac operator through the index theorem. In fact, the founders of QCD (see [10] for example) strongly suggested that the $SU(2)_L \times SU(2)_R$ breaking is triggered by the topologically nontrivial configuration of gluons and even quantitative estimate was made in [11]. However, this view of the $U(1)_A$ anomaly as the origin of the $SU(2)_L \times SU(2)_R$ breaking is not widely appreciated today since early lattice simulations reported survival of the axial $U(1)$ anomaly near the critical temperature, and thus, the $U(1)_A$ anomaly apparently gives little impact on the transition.

In this work, we revisit this issue, using lattice QCD with exactly chiral and flavor symmetric quarks. The index theorem is satisfied on the lattice to a good precision so that the relation between topological gauge excitation and fermion near-zero mode remains intact. By an eigenmode decomposition of the Dirac operator and quark propagators [12–15], we can unambiguously separate the $U(1)_A$ breaking effect from others in the chiral susceptibility $\chi(m) = \sum_x \langle S^0(x) S^0(0) \rangle - V \langle S^0(0) \rangle^2$. With the exact chiral symmetry, we can avoid severe lattice artifact that can induce large overestimate of the $U(1)_A$ breaking as demonstrated in [13, 14].

We find that $\chi(m)$ in the high temperature phase mostly probes the presence/absence of the $U(1)_A$ symmetry: the connected part is dominated by the $U(1)_A$ susceptibility defined as $\sum_x \langle P^a(x) P^a(0) - S^a(x) S^a(0) \rangle$, where $S^a(x)$ and $P^a(x)$ are iso-triplet scalar and pseudo-scalar operators, and the disconnected part is governed by the topological susceptibility, which measures the instanton number variance. Meanwhile, the $SU(2)_L \times SU(2)_R$ susceptibilities remain small even when the chiral condensate and $U(1)_A$ susceptibility become non-zero due to finite quark masses.

This result suggests a possibility that the chiral phase transition is actually driven by the $U(1)_A$ breaking as suggested in the early stage of QCD. In [16], it was argued that if the $U(1)_A$ breaking is kept large at the critical temperature the transition is likely to be the second order. But if the $U(1)_A$ symmetry effectively “emerges”, the order or the universality class of the transition differs from the naive expectation, which would require changes in the current understanding of the early universe.

2 Dirac eigenmode decomposition of susceptibilities

Let us start with the N_f -flavor QCD partition function with a nonzero vacuum angle θ ,

$$Z(m, \theta) = \int [dA] \det(D(A) + m)^{N_f} e^{-S_G(A) + i\theta Q(A)}, \quad (1)$$

where the path integral over the gauge field A is performed with a weight given by the gauge action $S_G(A)$, topological charge $Q(A)$, or equivalently the index of the Dirac operator $D(A)$, and the fermion determinant with a degenerate quark mass m . We have used a continuum notation for simplicity. The lattice formulas in terms of the overlap-Dirac operator [17] will be given later.

Denoting the eigenvalues of $D(A)$ by $i\lambda(A)$, among which every nonzero mode appears in a pair with its conjugate $-i\lambda(A)$, the chiral condensate at $\theta = 0$ is decomposed as

$$\Sigma(m) = \frac{1}{N_f V} \frac{\partial}{\partial m} \ln Z(m, 0) = \frac{1}{V} \left\langle \sum_{\lambda(A)} \frac{m}{\lambda(A)^2 + m^2} \right\rangle. \quad (2)$$

Here and in the following, the expectation value of a quantity $X(A)$ (with $\theta = 0$) is written as $\langle X(A) \rangle$.

The chiral susceptibility, defined as a derivative of $\Sigma(m)$ with respect to m , may be decomposed into two parts. The “connected” susceptibility $\chi^{\text{con.}}(m)$ is a derivative of the chiral condensate with respect to the valence quark mass m_v , while the “disconnected” part $\chi^{\text{dis.}}(m)$ is that with respect to the sea quark mass m_s , both with setting $m_v = m_s = m$ after all.

In the connected susceptibility, we have a term $\Sigma(m)/m$, which is a unique source of a quadratic divergence, while other pieces are only logarithmically divergent. To remove this quadratic divergence, we introduce a subtracted condensate $\Sigma_{\text{sub.}}(m)$,

$$\begin{aligned} \frac{\Sigma_{\text{sub.}}(m)}{m} &= \left[\frac{\Sigma(m)}{m} - \frac{\langle |Q(A)| \rangle}{m^2 V} \right] \\ &\quad - \left[\frac{\Sigma(m_{\text{ref}})}{m_{\text{ref}}} - \frac{\langle |Q(A)| \rangle|_{m=m_{\text{ref}}}}{m_{\text{ref}}^2 V} \right], \end{aligned} \quad (3)$$

with a reference quark mass m_{ref} . The term with $|Q(A)|$ eliminates the contribution from chiral zero modes, which is expected to vanish in the large V limit.

The connected susceptibility (with the subtraction above) can be written as

$$\chi_{\text{sub.}}^{\text{con.}}(m) = -\Delta_{U(1)}^{\text{con.}}(m) + \frac{\Sigma_{\text{sub.}}(m)}{m} + \frac{\langle |Q(A)| \rangle}{m^2 V}, \quad (4)$$

where

$$\Delta_{U(1)}^{\text{con.}}(m) = \frac{1}{V} \left\langle \sum_{\lambda(A)} \frac{2m^2}{(\lambda(A)^2 + m^2)^2} \right\rangle \quad (5)$$

is equivalent to the axial $U(1)$ susceptibility $\sum_x [\langle P^a(x)P^a(0) \rangle - \langle S^a(x)S^a(0) \rangle]$. (See [13, 14] for the details). On the other hand, the eigenvalue decomposition of the disconnected part is

$$\chi^{\text{dis.}}(m) = \frac{N_f}{V} \left[\left\langle \left(\sum_{\lambda(A)} \frac{m}{\lambda(A)^2 + m^2} \right)^2 \right\rangle - (\Sigma(m)V)^2 \right]. \quad (6)$$

From the θ dependence of $Z(m, \theta)$, we obtain the topological susceptibility,

$$\chi_t(m) = -\frac{1}{V} \frac{\partial^2}{\partial \theta^2} \ln Z(m, \theta) \Big|_{\theta=0} = \frac{\langle Q(A)^2 \rangle - \langle Q(A) \rangle^2}{V}. \quad (7)$$

Absorbing the angle θ to the mass term $m \rightarrow m \exp(i\gamma_5 \theta / N_f)$, we can relate $\chi_t(m)$ to the chiral condensate and the pseudoscalar susceptibility $\sum_x \langle P^0(x)P^0(0) \rangle$:

$$\chi_t(m) = m \left[\frac{\partial}{\partial \theta} \langle \bar{q} i \gamma_5 e^{i\gamma_5 \theta / N_f} q \rangle_{\theta} \right] \Big|_{\theta=0} = -\sum_x \langle P^0(x)P^0(0) \rangle - \frac{\Sigma(m)}{m}. \quad (8)$$

We can now see that the $U(1)_A$ and $SU(2)_L \times SU(2)_R$ symmetries are intimately related [18, 19]. Two possible probes of the $SU(2)_L \times SU(2)_R$ symmetry given by

$$\Delta_{SU(2)}^{(1)}(m) \equiv \sum_x \langle S^0(x)S^0(0) - P^a(x)P^a(0) \rangle - V \langle S^0(0) \rangle^2 = \chi^{\text{dis.}}(m) - \Delta_{U(1)}^{\text{con.}}(m), \quad (9)$$

$$\Delta_{SU(2)}^{(2)}(m) \equiv \sum_x \langle S^a(x)S^a(0) - P^0(x)P^0(0) \rangle = \frac{N_f}{m^2} \chi_t(m) - \Delta_{U(1)}^{\text{con.}}(m), \quad (10)$$

are actually written using the $U(1)_A$ related quantities $\Delta_{U(1)}^{\text{con.}}(m)$, $\chi_t(m)$ and $\chi^{\text{dis.}}(m)$. When the axial $U(1)$ anomaly is active so that $\Delta_{U(1)}^{\text{con.}}(m)$ [20–26] is nonzero, the recovery of the $SU(2)_L \times SU(2)_R$ requires a fine tuning

$$\lim_{m \rightarrow 0} \chi^{\text{dis.}}(m) = \lim_{m \rightarrow 0} \Delta_{U(1)}^{\text{con.}}(m) = \lim_{m \rightarrow 0} \frac{N_f}{m^2} \chi_t(m), \quad (11)$$

which is highly nontrivial.

From Eqs.(4), (9) and (10), we can separate the $U(1)_A$ breaking contributions $\chi_A^{\text{con.}}(m)$ and $\chi_A^{\text{dis.}}(m)$ from the connected and disconnected parts of the chiral susceptibility, $\chi_{\text{sub.}}^{\text{con.}}(m)$ and $\chi^{\text{dis.}}(m)$ respectively, as

$$\chi_A^{\text{con.}}(m) = -\Delta_{U(1)}^{\text{con.}}(m) + \frac{\langle |Q(A)| \rangle}{m^2 V}, \quad (12)$$

$$\chi_A^{\text{dis.}}(m) = \frac{N_f}{m^2} \chi_t(m). \quad (13)$$

Then the remnants are $\chi_{\text{sub.}}^{\text{con.}}(m) - \chi_A^{\text{con.}}(m) = \Sigma_{\text{sub.}}(m)/m$ and $\chi^{\text{dis.}}(m) - \chi_A^{\text{dis.}}(m) = \Delta_{SU(2)}^{(1)}(m) - \Delta_{SU(2)}^{(2)}(m)$, respectively.

These formulas can be promoted to those of lattice QCD with the overlap fermion [13]. Denoting the eigenvalue of massive overlap-Dirac operator $\gamma_5((1-m)D_{\text{ov}} + m)$ by λ_m , the eigenvalue decomposition can be obtained by replacing $\frac{1}{\lambda(A)^2 + m^2}$ by $\frac{(1-\lambda_m^2)}{(1-m^2)\lambda_m^2}$ (Here and in the following, we take the lattice spacing unity). In the following we numerically study how much the $U(1)_A$ -related pieces $\chi_A^{\text{con./dis.}}(m)$ dominate the signal of the chiral susceptibility in $N_f = 2$ lattice QCD. We employ a lattice fermion formulation that precisely preserves chiral symmetry, which is essential in the above formulas with spectral decomposition.

3 Lattice simulation

We use the gauge field ensembles generated in [15]. We employ the tree-level improved Symanzik gauge action and the Möbius domain-wall fermion [27] action for the simulations. We include the overlap fermion determinant utilizing a reweighting technique in order to eliminate systematics due to any violation of the chiral symmetry, as well as those due to the mixed action. The lattice spacing is fixed to $a = 0.074$ fm, and four different temperatures are chosen taking a set of the temporal lattice extent $L_t = 8, 10, 12$ and 14 , which covers $190 \leq T \leq 330$ MeV. We fix the lattice size to $L = 32$, which corresponds to 2.4 fm. At $T = 220$ MeV, three different lattice sizes $L = 24, 32, 40$ are taken in order to check if the finite volume effect is under control. The range of quark mass covers the physical up and down quark mass, estimated to be $m = 0.0014(2)$ from the pion mass $m_\pi = 0.135(8)$ at $T = 0$ and $m = 0.01$. We use the $m = 0.005$, which is the highest quark mass at $T = 190$ MeV simulations, on $L = 32$ lattices as the reference point m_{ref} for the subtraction of the connected chiral susceptibility.

We compute 40 lowest eigenvalues of the massive overlap-Dirac operator, as well as those of four-dimensional effective operator of the Möbius domain-wall fermion. For both operators, we can identify the index $Q(A)$ as the number of isolated chiral zero modes. At the lowest temperature, the 40th eigenvalue is ~ 0.08 (~ 210 MeV).

Since the number of stored eigenvalues is limited, we truncate the summation in the spectral decomposition of the chiral susceptibilities. In Fig.1, we plot the cut-off dependence of the (subtracted) chiral susceptibilities. We find for $T \leq 260$ MeV, both $\chi_{\text{sub.}}^{\text{con.}}$ and $\chi^{\text{dis.}}$ with the reweighted overlap fermion show a good saturation already at $\lambda = 0.07$ in all the simulated ensembles. At $T = 260$ MeV, we also find a good agreement with a full measurement without the truncation computed with the Möbius domain-wall Dirac operator. At $T = 330$ MeV, on the other hand, the low-mode approximation does not reproduce the full result especially at heavier quark masses. In our previous study [15] we found that at this temperature the low-lying modes are almost absent and the observables are insensitive to the violation of the lattice chiral symmetry. Therefore, in the following analysis at $T = 330$ MeV, we take the full computation with the Möbius domain-wall Dirac operator and use the low-mode approximation of the overlap-Dirac fermion at $\lambda_{\text{cut}} = 0.07$ (~ 180 MeV) for other ensembles of $T \leq 260$ MeV.

The statistical uncertainty is estimated by the jackknife method after binning the data in every 1000 trajectories with which the autocorrelation is negligible.

4 Numerical results

We summarize our numerical results in Tab. 1.

In Fig. 2, we present the results for the connected part $\chi_{\text{sub.}}^{\text{con.}}$ (top panel) and disconnected data $\chi^{\text{dis.}}$ (bottom) of the chiral susceptibility at $T = 220$ MeV on the $L = 32$ lattice (open squares). The filled symbols are those of $\chi_A^{\text{con.}}$ and $\chi_A^{\text{dis.}}$, which dominate the signals. The other contributions $\Sigma_{\text{sub.}}(m)/m$ (circles) and the $SU(2)$ susceptibilities $\Delta_{SU(2)}^{(1,2)}(m)$ (circles and triangles) are relatively small. This result indicates that the connected part of the subtracted chiral susceptibility is essentially described by the axial $U(1)$ susceptibility and the disconnected susceptibility is governed by the topological susceptibility¹. The axial $U(1)$ breaking contributions $\chi_A^{\text{con.}}$ and $\chi_A^{\text{dis.}}$ are strongly suppressed at the lightest quark mass. In the data with different lattice sizes $L = 24$ (crosses) and 40 (stars), no significant volume dependence is seen. The data may indicate a peak at $m = 0.005$.

These features are seen at all simulated temperatures and quark masses ranging from the physical point to $m \sim 100$ MeV. Figure 3 summarizes the quark mass dependence of the connected (top panel) and disconnected (bottom) chiral susceptibility at four different temperatures on the $L = 32$ lattices. The open symbols with solid lines are the data obtained

¹It was pointed out in [22, 25] that $\chi^{\text{dis.}}$ is dominated by the $U(1)_A$ breaking in the $m = 0$ limit, but the concrete form (in terms of the topological susceptibility) at finite m was not discussed.

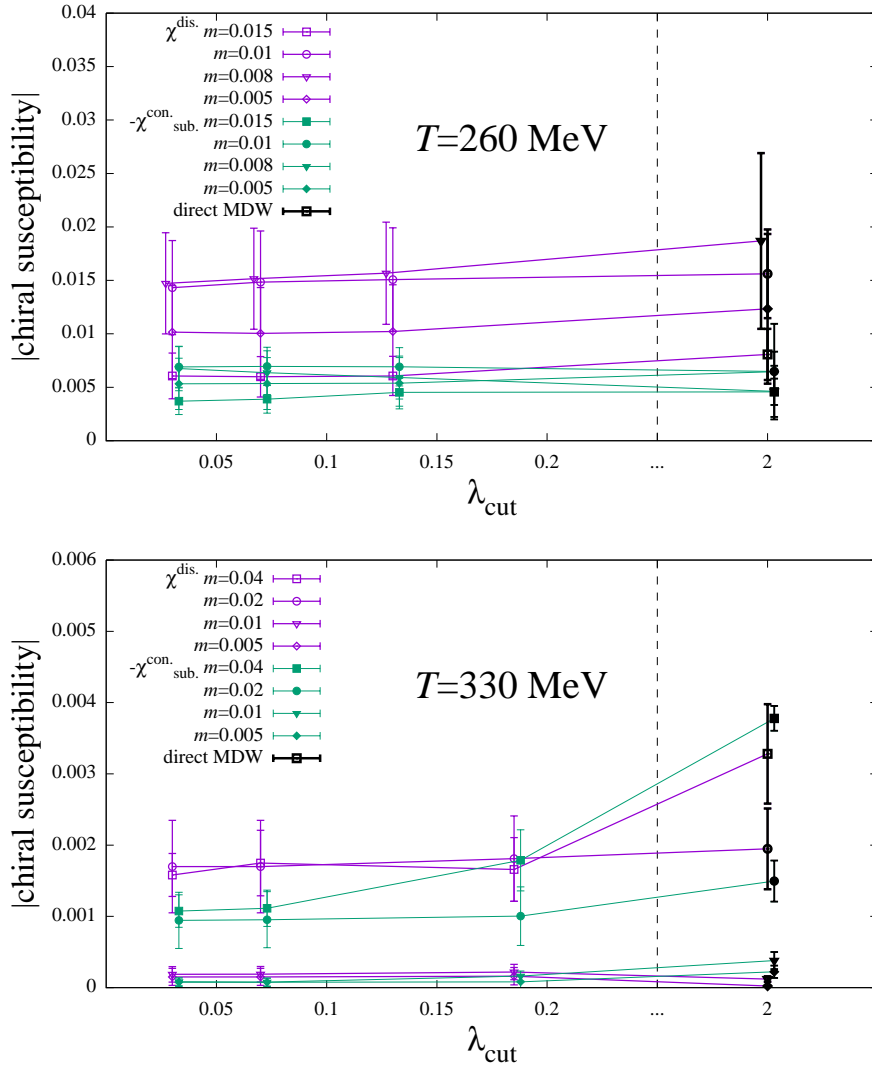


Fig. 1 Cut-off λ_{cut} dependence of the chiral susceptibility at $T = 260$ MeV (top panel) and $T = 330$ MeV (bottom). The result for $\chi^{\text{dis.}}$ is plotted by open symbols, while that for $-\chi^{\text{con.}}_{\text{sub.}}$ is shown by filled symbols. The thick symbols plotted at the lattice cut-off = 2 denote those obtained from the direct inversion of the Möbius domain-wall operator.

from the eigenmode decomposition of the reweighted overlap-Dirac operator, while those with dotted lines are from direct measurement with the Möbius domain-wall fermion. At each temperature, the axial $U(1)$ breaking effect $\chi_A^{\text{con.}/\text{dis.}}$ (filled symbols with dashed lines) dominates the signal of the susceptibility. It is remarkable that this dominance is seen even at higher quark mass region than the peaks, where both $SU(2)_L \times SU(2)_R$ and $U(1)_A$ are expected to be sizably broken. In fact, we find that a simple sums of $\chi_A^{\text{con.}}$ and $\chi_A^{\text{dis.}}$ over 26 simulated data points are $-0.48(2)$ and $0.74(6)$, respectively, while those of $\chi^{\text{con.}}_{\text{sub.}}$ and $\chi^{\text{dis.}}$

$T(\text{MeV})$	$L^3 \times L_t$	m	$\chi_{\text{sub.}}^{\text{con.}}$	$\chi_A^{\text{con.}}$	$\chi^{\text{dis.}}$	$\chi_A^{\text{dis.}}$	
190	$32^3 \times 14$	0.005	-0.074(07)	-0.074(12)	0.090(12)	0.077(17)	
		0.00375	-0.101(20)	-0.106(26)	0.144(39)	0.189(49)	
		0.0025	-0.058(12)	-0.056(11)	0.087(15)	0.079(21)	
		0.001	-0.0188(64)	-0.00130(45)	0.0020(06)	1.6(16)e-7	
220	$24^3 \times 12$	0.01	-0.0224(23)	-0.0202(34)	0.0399(75)	0.0338(68)	
		0.005	-0.0367(87)	-0.0332(88)	0.066(20)	0.072(24)	
		0.00375	-0.0081(28)	-0.0041(27)	0.0079(52)	0.0070(53)	
		0.0025	-0.0125(55)	-0.0095(54)	0.019(11)	0.018(11)	
		0.001	-0.0033(25)	-0.0002(01)	0.00033(24)	0(0)	
	$32^3 \times 12$	0.01	-0.0284(25)	-0.0325(38)	0.044(07)	0.049(11)	
		0.005	-0.0311(42)	-0.0311(48)	0.065(11)	0.068(14)	
		0.00375	-0.00682(83)	-0.00270(70)	0.0050(13)	0.0038(13)	
		0.0025	-0.0073(49)	-0.0062(48)	0.0121(94)	0.0112(95)	
		0.001	-0.0016(12)	-0.00016(06)	0.00030(12)	1.8(18)e-5	
	$40^3 \times 12$	0.01	-0.0270(15)	-0.0349(28)	0.0417(56)	0.0397(49)	
		0.005	-0.0305(31)	-0.0371(56)	0.0526(65)	0.0433(54)	
	260	$32^3 \times 10$	0.015	-0.0039(13)	-0.0038(14)	0.0060(19)	0.0061(24)
			0.01	-0.0070(18)	-0.0077(24)	0.0148(48)	0.0141(43)
			0.008	-0.0064(20)	-0.0089(32)	0.0152(47)	0.0117(38)
			0.005	-0.0054(24)	-0.0054(24)	0.0100(43)	0.0103(45)
330	$32^3 \times 8$	0.040	-0.00378(17)	-0.00306(21)	0.00328(70)	0.00219(40)	
		0.020	-0.00150(29)	-0.00145(30)	0.00195(57)	0.00148(49)	
		0.015	-0.00145(65)	-0.00151(82)	0.0027(19)	0.0017(11)	
		0.01	-0.000386(95)	-0.000183(62)	0.00012(03)	0.00044(31)	
		0.005	-0.000222(87)	-0.000222(77)	2.33(53)e-5	0(0)	
		0.001	-0.00010(10)	-2.81(58)e-5	8.6(14)e-7	0(0)	

Table 1 Summary of results

are $-0.50(2)$ and $0.73(4)$. They differ by only 3% and 1% and within standard deviation. Also, we note that the axial $U(1)$ breaking contributions are strongly suppressed near the chiral limit.

We also plot the result obtained in our previous work with $\beta = 4.24$ on a coarser lattice ($a=0.084$ fm) at $T = 195$ MeV (cross symbols). The result is consistent with our new data at a similar temperature $T = 190$ MeV, which indicates that the cut-off effect is not significant.

In Fig. 3 the position of the peak moves towards heavier quark masses as temperature increases. It indicates that our simulated temperatures cover the pseudo-critical temperature, which becomes higher for larger quark masses².

In the total contribution $\chi_{\text{sub.}}^{\text{con.}}(m) + \chi^{\text{dis.}}(m)$, however, the situation is not so simple. As shown in Fig. 4, the $U(1)_A$ breaking dominance by

$$\chi_A^{\text{con.}}(m) + \chi_A^{\text{dis.}}(m) = -\Delta_{U(1)}^{\text{con.}}(m) + \frac{N_f}{m^2}\chi_t(m) + \frac{\langle|Q(A)|\rangle}{m^2V}, \quad (14)$$

is still visible. But the smallness of $\Delta_{SU(2)}^{(1),(2)}(m)$ implies $\Delta_{U(1)}^{\text{con.}}(m) \sim \frac{N_f}{m^2}\chi_t(m)$ so that the quantity is dominated by the last term $\frac{\langle|Q(A)|\rangle}{m^2V}$, which is expected to vanish in the thermodynamical limit. Therefore, in order to quantify the axial $U(1)$ breaking effect in the total contribution, we need a careful analysis of the delicate cancellation between $\Delta_{U(1)}^{\text{con.}}(m)$ and $\frac{N_f}{m^2}\chi_t(m)$, as well as their large volume limits. Although such a fine analysis is beyond the scope of this work, let us try to raise two possible scenarios. The first one is that the signal of the total susceptibility gets smaller as the volume increases and it is eventually given by the tiny quark mass dependence of the $SU(2)_L \times SU(2)_R$ breaking. The second is that even when $\frac{\langle|Q(A)|\rangle}{m^2V}$ disappears in the large volume limit, the near-chiral-zero modes in $\Sigma_{\text{sub.}}(m)$ compensate its absence and keep the total susceptibility insensitive to the volume. In Fig. 5, we plot $\frac{\Sigma_{\text{sub.}}(m)}{m} + \frac{\langle|Q(A)|\rangle}{m^2V}$ (open and solid symbols) and $\frac{\langle|Q(A)|\rangle}{m^2V}$ (filled and dashed) as functions of the lattice size L . The consistency of the former at $L = 32$ and 40 in spite of the decrease of the latter may be a support of the second scenario.

We conclude that the connected and disconnected chiral susceptibilities are dominated by the axial $U(1)$ breaking effects at temperatures $T \gtrsim 190$ MeV, which covers the pseudo-critical temperature when the quark mass is finite. The connected part is described by the axial $U(1)$ susceptibility other than the m -independent quadratically divergent part, and the disconnected part is governed by the topological susceptibility. The chiral limit of the $U(1)_A$ contributions is strongly suppressed. The picture of QCD phase diagram [16], based on the spontaneous $SU(2)_L \times SU(2)_R$ breaking alone, may need to be reconsidered, or a delicate cancellation between the connected and disconnected parts of the $U(1)_A$ breaking is, at least, required. It is turned out that the axial $U(1)$ breaking does play a crucial role.

² A strong increase of the pseudo-critical temperature was reported in 2+1-flavor lattice QCD simulations [9].

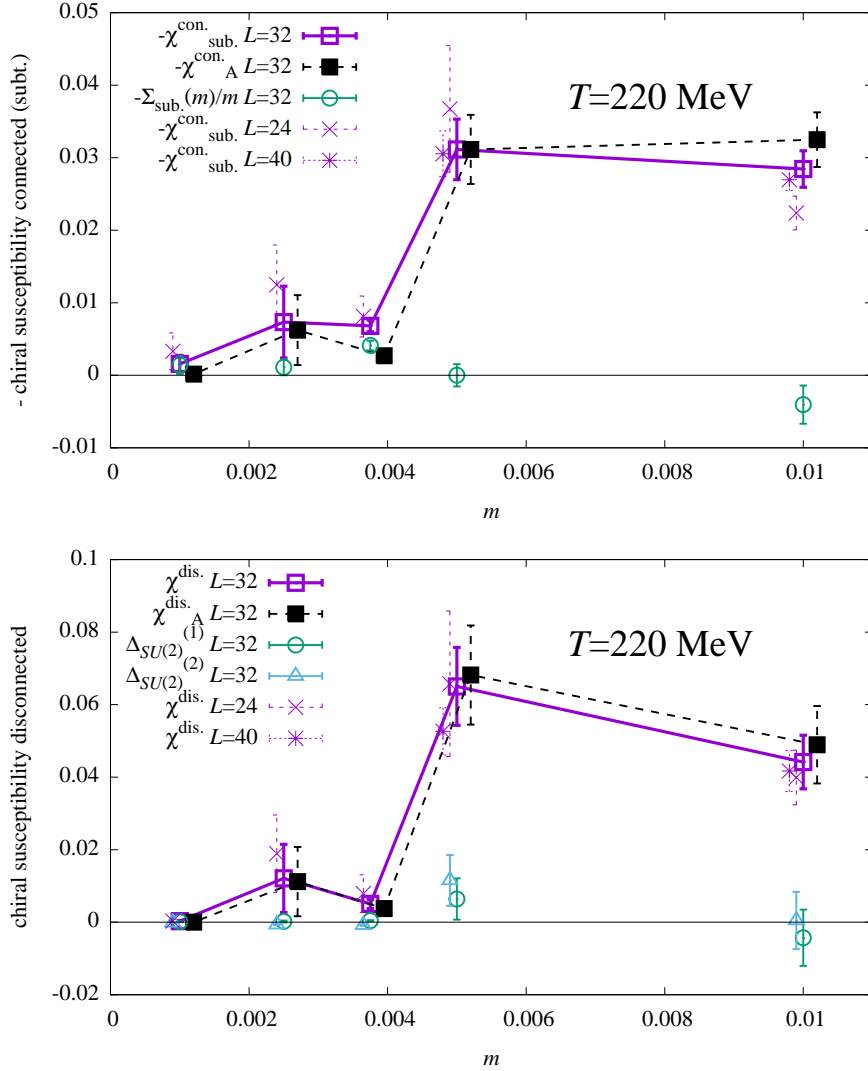


Fig. 2 Quark mass dependence of the connected (top panel) and disconnected (bottom) chiral susceptibilities on the $L = 32$ lattice (open squares). The contribution from the axial $U(1)$ breaking (filled squares) saturates the signal, while the remaining $\Sigma_{\text{sub.}}(m)/m$ and $\Delta_{SU(2)}^{(1,2)}(m)$ plotted by open circles and triangles are small. The $L = 24$ (crosses) and $L = 40$ (stars) data show no significant volume dependence. Note that the sign of the connected part is flipped.

Acknowledgment

We thank H.-T. Ding, C. Gattringer, L. Glozman, for useful discussions. We thank P. Boyle for correspondence for starting simulation with Grid and I. Kanamori for helping us on the simulations on K computer with Bridge++. We also thank the members of JLQCD

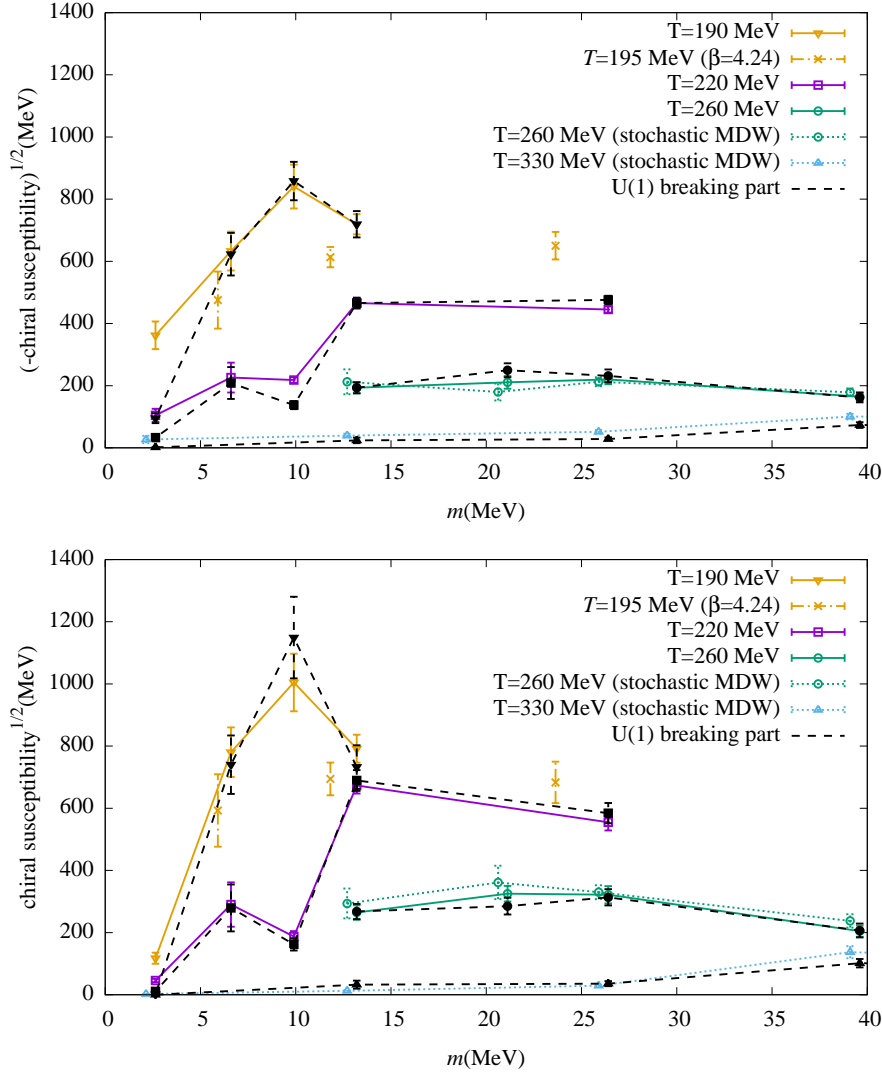


Fig. 3 Chiral susceptibility at four different temperatures on the $L = 32$ lattices (open symbols). The connected (top panel) and disconnected (bottom) parts are shown. The filled symbols are those from the axial $U(1)$ breaking.

collaboration for their encouragement and support. We thank the Yukawa Institute for Theoretical Physics at Kyoto University. Discussions during the YITP workshop YITP-W-20-08 on "Progress in Particle Physics 2020" were useful to complete this work. Numerical simulations were performed using the QCD software packages Iroiro++ [28], Grid [29], and Bridge++ [30] on IBM System Blue Gene Solution at KEK under a support of its Large Scale Simulation Program (No. 16/17-14) and Oakforest-PACS at JCAHPC under a support of the HPCI System Research Projects (Project IDs: hp170061, hp180061, hp190090, and hp200086), Multidisciplinary Cooperative Research Program in CCS, University of Tsukuba

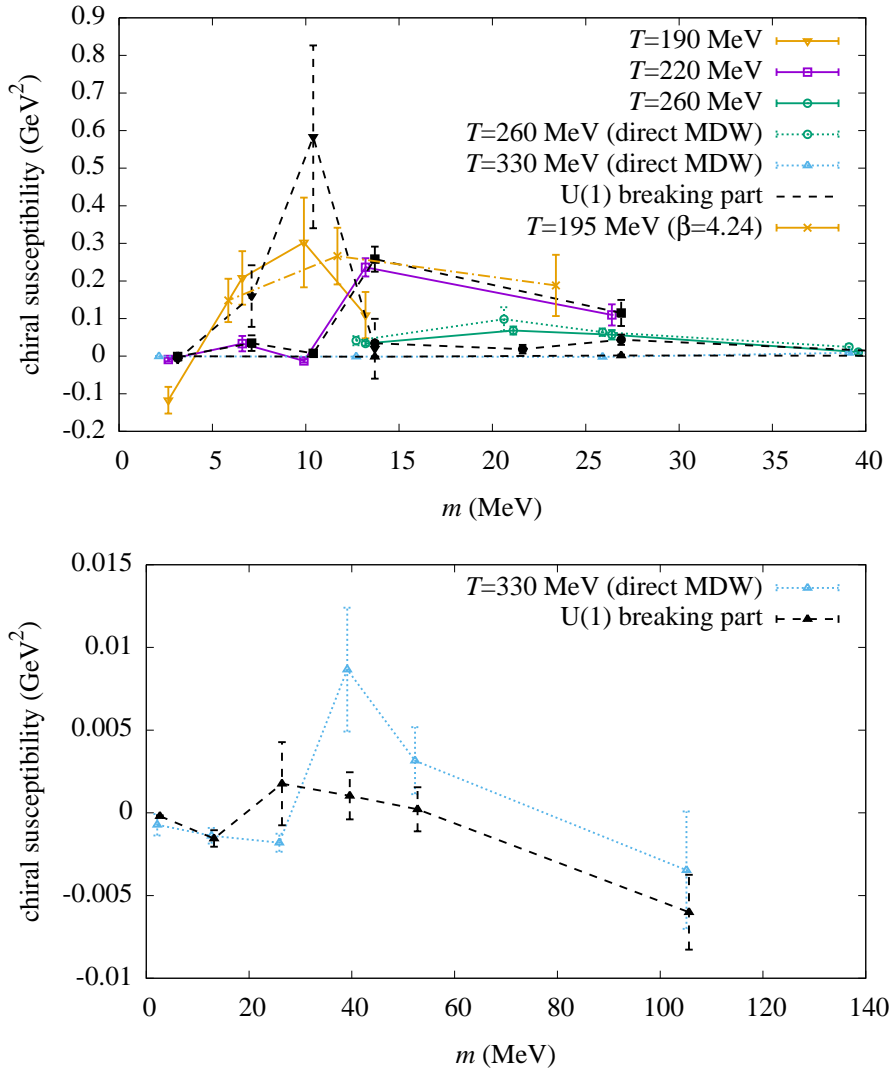


Fig. 4 Chiral susceptibility at four different temperatures on the $L = 32$ lattices (open symbols). The filled symbols are those from the axial $U(1)$ breaking. The bottom panel is the same plot as the top but the result at $T = 330$ MeV is shown in a fine scale.

(Project IDs: xg17i032 and xg18i023) and K computer provided by the RIKEN Center for Computational Science. We used Japan Lattice Data Grid (JLDG) [31] for storing a part of the numerical data generated for this work. This work is supported in part by the Japanese Grant-in-Aid for Scientific Research (No. JP26247043, JP16H03978, JP18H01216, JP18H03710, JP18H04484, JP18H05236), and by MEXT as “Priority Issue on Post-K computer” (Elucidation of the Fundamental Laws and Evolution of the Universe) and by Joint Institute for Computational Fundamental Science (JICFuS).

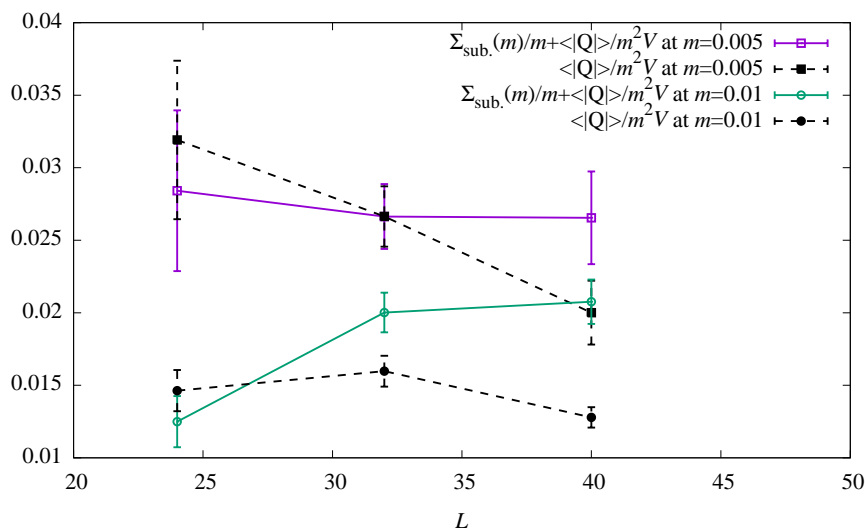


Fig. 5 The lattice size L dependence of $\frac{\Sigma_{\text{sub.}}(m)}{m} + \frac{\langle |Q(A)| \rangle}{m^2 V}$ (open symbols connected by solid lines) and $\frac{\langle |Q(A)| \rangle}{m^2 V}$ (filled symbols connected by dashed lines). The data at $m = 0.01$ and 0.005 are presented.

References

- [1] F. Karsch and E. Laermann, “Susceptibilities, the specific heat and a cumulant in two flavor QCD,” *Phys. Rev. D* **50**, 6954-6962 (1994) doi:10.1103/PhysRevD.50.6954 [arXiv:hep-lat/9406008 [hep-lat]].
- [2] Y. Aoki, G. Endrodi, Z. Fodor, S. D. Katz and K. K. Szabo, “The Order of the quantum chromodynamics transition predicted by the standard model of particle physics,” *Nature* **443**, 675-678 (2006) doi:10.1038/nature05120 [arXiv:hep-lat/0611014 [hep-lat]].
- [3] M. Cheng *et al.*, “The Transition temperature in QCD,” *Phys. Rev. D* **74**, 054507 (2006) doi:10.1103/PhysRevD.74.054507 [arXiv:hep-lat/0608013 [hep-lat]].
- [4] A. Bazavov *et al.* [HotQCD Collaboration], “The chiral and deconfinement aspects of the QCD transition,” *Phys. Rev. D* **85**, 054503 (2012) doi:10.1103/PhysRevD.85.054503 [arXiv:1111.1710 [hep-lat]].
- [5] T. Bhattacharya *et al.* [HotQCD Collaboration], “QCD Phase Transition with Chiral Quarks and Physical Quark Masses,” *Phys. Rev. Lett.* **113**, no.8, 082001 (2014) doi:10.1103/PhysRevLett.113.082001 [arXiv:1402.5175 [hep-lat]].
- [6] C. Bonati, M. D’Elia, M. Mariti, M. Mesiti, F. Negro and F. Sanfilippo, “Curvature of the chiral pseudocritical line in QCD: Continuum extrapolated results,” *Phys. Rev. D* **92**, no.5, 054503 (2015) doi:10.1103/PhysRevD.92.054503.
- [7] B. B. Brandt, A. Francis, H. B. Meyer, O. Philipsen, D. Robaina and H. Wittig, “On the strength of the $U_A(1)$ anomaly at the chiral phase transition in $N_f = 2$ QCD,” *JHEP* **12**, 158 (2016) doi:10.1007/JHEP12(2016)158 [arXiv:1608.06882 [hep-lat]].
- [8] Y. Taniguchi *et al.* [WHOT-QCD Collaboration], “Exploring $N_f = 2+1$ QCD thermodynamics from the gradient flow,” *Phys. Rev. D* **96**, no.1, 014509 (2017) [erratum: *Phys. Rev. D* **99**, no.5, 059904 (2019)] doi:10.1103/PhysRevD.96.014509 [arXiv:1609.01417 [hep-lat]].
- [9] H. T. Ding *et al.* [HotQCD Collaboration], “Chiral Phase Transition Temperature in (2+1)-Flavor QCD,” *Phys. Rev. Lett.* **123**, no.6, 062002 (2019) doi:10.1103/PhysRevLett.123.062002 [arXiv:1903.04801 [hep-lat]].
- [10] C. G. Callan, Jr., R. F. Dashen and D. J. Gross, “Toward a Theory of the Strong Interactions,” *Phys. Rev. D* **17**, 2717 (1978) doi:10.1103/PhysRevD.17.2717
- [11] D. Diakonov and V. Y. Petrov, “CHIRAL CONDENSATE IN THE INSTANTON VACUUM,” *Phys. Lett. B* **147**, 351-356 (1984) doi:10.1016/0370-2693(84)90132-1
- [12] S. Aoki, H. Fukaya and Y. Taniguchi, “Chiral symmetry restoration, eigenvalue density of Dirac operator and axial $U(1)$ anomaly at finite temperature,” *Phys. Rev. D* **86**, 114512 (2012) doi:10.1103/PhysRevD.86.114512

- [arXiv:1209.2061 [hep-lat]].
- [13] G. Cossu *et al.* [JLQCD Collaboration], “Violation of chirality of the Möbius domain-wall Dirac operator from the eigenmodes,” *Phys. Rev. D* **93**, no. 3, 034507 (2016) doi:10.1103/PhysRevD.93.034507 [arXiv:1510.07395 [hep-lat]].
- [14] A. Tomiya *et al.* [JLQCD Collaboration] “Evidence of effective axial U(1) symmetry restoration at high temperature QCD,” *Phys. Rev. D* **96**, no. 3, 034509 (2017) Addendum: [*Phys. Rev. D* **96**, no. 7, 079902 (2017)] doi:10.1103/PhysRevD.96.034509, 10.1103/PhysRevD.96.079902 [arXiv:1612.01908 [hep-lat]].
- [15] S. Aoki *et al.* [JLQCD Collaboration], “Study of axial U(1) anomaly at high temperature with lattice chiral fermions,” [arXiv:2011.01499 [hep-lat]].
- [16] R. D. Pisarski and F. Wilczek, “Remarks on the Chiral Phase Transition in Chromodynamics,” *Phys. Rev. D* **29**, 338 (1984) doi:10.1103/PhysRevD.29.338.
- [17] H. Neuberger, “Exactly massless quarks on the lattice,” *Phys. Lett. B* **417**, 141 (1998) doi:10.1016/S0370-2693(97)01368-3 [hep-lat/9707022].
- [18] A. Gómez Nicola and J. Ruiz De Elvira, “Chiral and $U(1)_A$ restoration for the scalar and pseudoscalar meson nonets,” *Phys. Rev. D* **98**, no.1, 014020 (2018) doi:10.1103/PhysRevD.98.014020 [arXiv:1803.08517 [hep-ph]].
- [19] A. G. Nicola, “Light quarks at finite temperature: chiral restoration and the fate of the $U(1)_A$ symmetry,” [arXiv:2012.13809 [hep-ph]].
- [20] A. Bazavov *et al.* [HotQCD Collaboration], “The chiral transition and $U(1)_A$ symmetry restoration from lattice QCD using Domain Wall Fermions,” *Phys. Rev. D* **86**, 094503 (2012) doi:10.1103/PhysRevD.86.094503 [arXiv:1205.3535 [hep-lat]].
- [21] G. Cossu, S. Aoki, H. Fukaya, S. Hashimoto, T. Kaneko, H. Matsufuru and J.-I. Noaki, “Finite temperature study of the axial U(1) symmetry on the lattice with overlap fermion formulation,” *Phys. Rev. D* **87**, no. 11, 114514 (2013) Erratum: [*Phys. Rev. D* **88**, no. 1, 019901 (2013)] doi:10.1103/PhysRevD.88.019901, 10.1103/PhysRevD.87.114514 [arXiv:1304.6145 [hep-lat]].
- [22] M. I. Buchoff *et al.* [LLNL/RBC Collaboration], “QCD chiral transition, $U(1)_A$ symmetry and the dirac spectrum using domain wall fermions,” *Phys. Rev. D* **89**, no.5, 054514 (2014) doi:10.1103/PhysRevD.89.054514 [arXiv:1309.4149 [hep-lat]].
- [23] V. Dick, F. Karsch, E. Laermann, S. Mukherjee and S. Sharma, “Microscopic origin of $U_A(1)$ symmetry violation in the high temperature phase of QCD,” *Phys. Rev. D* **91**, no. 9, 094504 (2015) doi:10.1103/PhysRevD.91.094504. [arXiv:1502.06190 [hep-lat]].
- [24] K.-I. Ishikawa, Y. Iwasaki, Y. Nakayama and T. Yoshie, “Nature of chiral phase transition in two-flavor QCD,” arXiv:1706.08872 [hep-lat].
- [25] H. T. Ding, S. T. Li, S. Mukherjee, A. Tomiya, X. D. Wang and Y. Zhang, “Correlated Dirac eigenvalues and axial anomaly in chiral symmetric QCD,” *Phys. Rev. Lett.* **126**, no.8, 082001 (2021) doi:10.1103/PhysRevLett.126.082001 [arXiv:2010.14836 [hep-lat]].
- [26] O. Kaczmarek, L. Mazur and S. Sharma, “Eigenvalue spectra of QCD and the fate of $U_A(1)$ breaking towards the chiral limit,” [arXiv:2102.06136 [hep-lat]].
- [27] R. C. Brower, H. Neff and K. Orginos, “Möbius fermions,” *Nucl. Phys. Proc. Suppl.* **153**, 191 (2006) doi:10.1016/j.nuclphysbps.2006.01.047 [hep-lat/0511031]; “The Möbius domain wall fermion algorithm,” *Comput. Phys. Commun.* **220**, 1 (2017) doi:10.1016/j.cpc.2017.01.024 [arXiv:1206.5214 [hep-lat]].
- [28] G. Cossu, J. Noaki, S. Hashimoto, T. Kaneko, H. Fukaya, P. A. Boyle and J. Doi, “JLQCD IroIro++ lattice code on BG/Q,” [arXiv:1311.0084 [hep-lat]].
- [29] P. Boyle, A. Yamaguchi, G. Cossu and A. Portelli, “Grid: A next generation data parallel C++ QCD library,” [arXiv:1512.03487 [hep-lat]].
- [30] S. Ueda, S. Aoki, T. Aoyama, K. Kanaya, H. Matsufuru, S. Motoki, Y. Namekawa, H. Nemura, Y. Taniguchi and N. Ukita, “Development of an object oriented lattice QCD code ‘Bridge++’,” *J. Phys. Conf. Ser.* **523**, 012046 (2014) doi:10.1088/1742-6596/523/1/012046
- [31] T. Amagasa, S. Aoki, Y. Aoki, T. Aoyama, T. Doi, K. Fukumura, N. Ishii, K. I. Ishikawa, H. Jitsumoto and H. Kamano, *et al.* “Sharing lattice QCD data over a widely distributed file system,” *J. Phys. Conf. Ser.* **664**, no.4, 042058 (2015) doi:10.1088/1742-6596/664/4/042058

A Comparison with Ding *et al.* [25]

Recently, Ding *et al.* [25] investigated the disconnected part of chiral susceptibility in $N_f = 2 + 1$ QCD using eigenvalues of the Dirac operator of highly improved staggered quark

(HISQ) action. At $T = 207$ MeV they obtained a non-zero continuum limit, which suggests that the axial $U(1)$ symmetry is still broken by anomaly at $1.6 T_c$. As their conclusion qualitatively differs from ours, which becomes consistent with zero at the lightest simulated quark mass, here we would like to compare the two.

In Fig. A1 we present the data of [25] with open symbols and that of this work with the filled symbols. Since the strange quark is quenched in our simulations, we simply use the physical value of the strange quark mass for m_s . Note that the critical temperature is estimated to be ~ 130 MeV for $N_f = 2 + 1$ QCD while it is ~ 170 MeV for $N_f = 2$. Interestingly, a qualitative feature of sharp drops towards the chiral limit is similar. However, a significant cutoff $1/a$ dependence is seen in [25] the data at $a = 0.06$ fm are twice larger than those at $a = 0.08$ fm, while our data at $a = 0.08$ fm ($T = 195$ MeV) and those at $a = 0.07$ fm ($T = 190$ MeV) do not show such a sizable discretization effect.

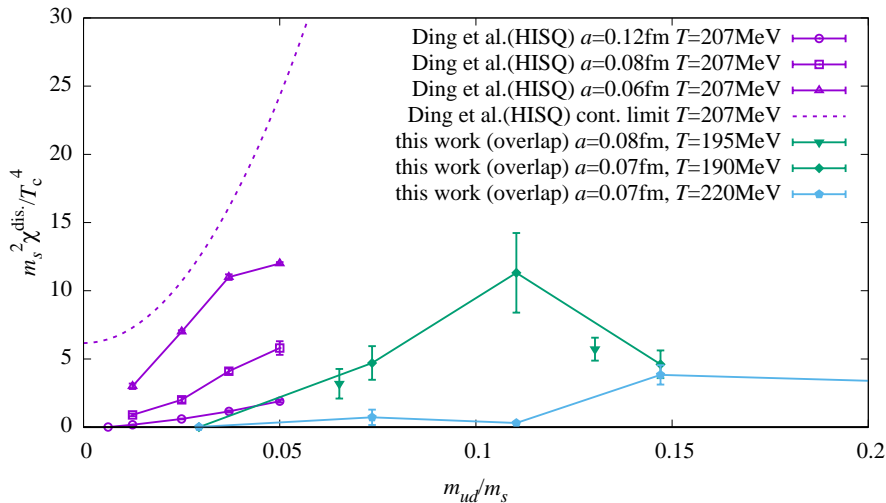


Fig. A1 Comparison of $\chi^{\text{dis.}}(m)$ between Ding *et al.* [25] (open symbols) and this work (filled). A qualitative feature of the sharp drop towards the chiral limit is similar. But the large scaling violation in [25] leads to a continuum limit much larger than the raw values as shown in the dashed curve.

In [25] they obtained a continuum limit with a global fit with 6 parameters, which is shown by the dashed curve in Fig. A1. It is clearly higher than the raw data at finite lattice spacings. Specifically, the one at the second lightest quark mass at $a = 0.12$ fm is extrapolated to a continuum limit that is 40 times larger, which suggests that their lattice data are not on a proper scaling trajectory that allows continuum extrapolation assuming an expansion in a^2 . Since the $U(1)_A$ anomaly does not correctly couple to the taste singlet component of the

staggered fermion that [25] employed, the quantities which are highly affected by the chiral anomaly and index theorem may receive large discretization effects in their simulation.